Quantum-dot-conjugated graphene oxide as an optical tool for biosensor

Erin Jenrette, Sangram K. Pradhan, Gugu Rutherford, Jasmin Flowers, Duc Ha, and Aswini K. Pradhan*

Center for Materials Research, Norfolk State University, 700 Park Ave., Norfolk, VA 23504, USA
**apradhan@nsu.edu*

Abstract: We have demonstrated a novel platform of quantum dots (QDs) core-shell conjugated graphene oxide (GO) biosensor for effective protein detection. The advantage in making core shell nanostructure allows preserving stable QDs, by improving quantum yield, and lowering the toxicity of the core. Both QDs and GO are efficient nanoparticle systems that can potentially be used for drug delivery, diagnosis, and biosensors scaffolds. However, our study indicates that the conjugation between these two nanoparticle systems makes their properties even more effective. The change in fluorescent intensity through fluorescence resonance energy transfer from quantum dots to GO produced a novel method for detection of the target and allows for the optimization of the recognition limit of Bovine serum albumin (BSA) due to efficient fluorescence resonance energy transfer as observed through time resolved relaxation spectroscopy. It is observed that the quenching of photoluminescence peak of QDs due to GO shell produced an applicable strategy and could be conveniently extended for detection of other biomolecules. We obtained significantly enhanced spectral signal through successful conjugation of GO with CdSe/CdS core shell, which can potentially be used for the detection of biomolecules with high sensitivity and selectivity. Our study underlines the efficiency of QD conjugated GO core shell in spectral detection of proteins even at very low concentration (0.25 mmol).

OCIS codes: (170.5660) Raman spectroscopy; (260.3800) Luminescence; (160.4236) Nanomaterials;

References and links

1. D. M. Good, V. Thongboonkerd, J. Novak, J. L. Bascands, J. P. Schanstra, J. J. Coon, A. Dominiczak, and H. Mischak, "Body fluid proteomics for biomarker discovery: lessons from the past hold the key to success in the future," J. Proteome Res. **6**(12), 4549–4555 (2007).
2. F. Gentile, G. Das, M. L. Coluccio, F. Mecarini, A. Accardo, L. Tirinato, R. Tallerico, G. Cojoc, C. Liberale, P. Candeloro, P. Decuzzi, F. De Angelis, and E. Di Fabrizio, "Ultra lowconcentrated molecular detection using super hydrophobic surface based biophotonicdevices," Microelectron. Eng. **87**(5-8), 798–801 (2010).
3. A. Sahu, K. Dalal, S. Naglot, P. Aggarwal, and C. Murali Krishna, "Serum Based Diagnosis of Asthma Using Raman Spectroscopy: An Early Phase Pilot Study," PLoS One **8**(11), e78921 (2013).
4. C. H. Lu, H. H. Yang, C. L. Zhu, X. Chen, and G. N. Chen, "A graphene platform for sensing biomolecules," Angew. Chem. Int. Ed. Engl. **48**(26), 4785–4787 (2009).
5. K. S. Novoselov, A. K. Geim, S. V. Morozov, D. Jiang, Y. Zhang, S. V. Dubonos, I. V. Grigorieva, and A. A. Firsov, "Electric field effect in atomically thin carbon films," Science **306**(5696), 666–669 (2004).
6. K. S. Novoselov, A. K. Geim, S. V. Morozov, D. Jiang, M. I. Katsnelson, I. V. Grigorieva, S. V. Dubonos, and A. A. Firsov, "Two-dimensional gas of massless Dirac fermions in graphene," Nature **438**(7065), 197–200 (2005).
7. H. Shen, L. Zhang, M. Liu, and Z. Zhang, "Biomedical Applications of Graphene," Theranostics **2**(3), 283–294 (2012).
8. G. Lu, K. Yu, Z. Wen, and J. Chen, "Semiconducting graphene: converting graphene from semimetal to semiconductor," Nanoscale **5**(4), 1353–1368 (2013).
9. L. Tang, Y. Wang, and J. Li, "The graphene/nucleic acid nanobiointerface," Chem. Soc. Rev. (2015) in press.

#246749 Received 27 Jul 2015; revised 9 Sep 2015; accepted 9 Sep 2015; published 15 Sep 2015

10. H. Qiu, N. Wu, Y. Zheng, M. Chen, S. Weng, Y. Chen, and X. Lin, "A robust and versatile signal-on fluorescence sensing strategy based on SYBR Green I dye and graphene oxide," Int. J. Nanomedicine **10**, 147–156 (2015).
11. I. L. Medintz, H. T. Uyeda, E. R. Goldman, and H. Mattoussi, "Quantum dot bioconjugates for imaging, labelling and sensing," Nat. Mater. **4**(6), 435–446 (2005).
12. R. J. Martín-Palma, M. Manso, and V. Torres-Costa, "Optical biosensors based on semiconductor nanostructures," Sensors (Basel) **9**(7), 5149–5172 (2009).
13. H. Dong, W. Gao, F. Yan, H. Ji, and H. Ju, "Fluorescence resonance energy transfer between quantum dots and graphene oxide for sensing biomolecules," Anal. Chem. **82**(13), 5511–5517 (2010).
14. A. M. Smith, S. Nie, "Semiconductor nanocrystals: structure, properties, and band gap engineering," Acc. Chem. Res. **43**(2), 190–200 (2010).
15. W. Fritzsche and J. Popp, "Optical nano- and microsystems forbioanalytics series: springer series on chemical sensors and biosensors," **10**, XII, p-329 (Eds.) (2012).
16. J. M. Reyes-Goddard, H. Barr, and N. Stone, "Photodiagnosis using Raman and surface enhanced Raman scattering of bodily fluids," Photodiagn. Photodyn. Ther. **2**(3), 223–233 (2005).
17. S. Schlücker, *Surface Enhanced Raman Spectroscopy: Analytical, Biophysicaland Life Science Applications* (Wiley-VCH, 2011)
18. Z. Liu, Z. Guo, H. Zhong, X. Qin, M. Wan, and B. Yang, "Graphene oxide based enhanced Raman Scattering probes for cancer cell imaging," Phys. Chem. Chem. Phys. **15**(8), 2961–2966 (2013).
19. S. He, K.-K. Liu, S. Su, J. Yan, X. Mao, D. Wang, Y. He, L.-J. Li, S. Song, and C. Fan, "Graphene-Based High-Efficiency Surface-Enhanced Raman Scattering-Active Platform for Sensitive and Multiplex DNA Detection," Anal. Chem. **84**(10), 4622–4627 (2012).
20. A. Cao, Z. Liu, S. Chu, M. Wu, Z. Ye, Z. Cai, Y. Chang, S. Wang, Q. Gong, and Y. Liu, "A Facile One-Step Method to Produce Graphene-CdS Quantum Dot Nanocomposites as Promising Optoelectronic Materials," Adv. Mater. **22**(1), 103–106 (2010).
21. J. J. Li, Y. A. Wang, W. Guo, J. C. Keay, T. D. Mishima, M. B. Johnson, and X. Peng, "Large-scale synthesis of nearly monodisperse CdSe/CdS core/shell nanocrystals using air-stable reagents via successive ion layer adsorption and reaction," J. Am. Chem. Soc. **125**(41), 12567–12575 (2003).
22. O. Chen, X. Chen, Y. Yang, J. Lynch, H. Wu, J. Zhuang, and Y. C. Cao, "Synthesis of metal-selenide nanocrystals using selenium dioxide as the selenium precursor," Angew. Chem. Int. Ed. Engl. **47**(45), 8638–8641 (2008).
23. W. S. Hummers, Jr. and R. E. Offeman, "Preparation of graphitic oxide," J. Am. Chem. Soc. **80**(6), 1339 (1958).
24. D. Yu, K. Park, M. Durstock, and L. Dai, "Fullerene-Grafted Graphene for Efficient Bulk Heterojunction Polymer Photovoltaic Devices," J. Phys. Chem. Lett. **2**(10), 1113–1118 (2011).
25. Y. F. Chen, T. H. Ji, and Z. Rosenzweig, "Synthesis of Glyconanospheres Containing Luminescent CdSe–ZnS Quantum Dots," Nano Lett. **3**(5), 581–584 (2003).
26. F. Hua, M. T. Swihart, and E. Ruckenstein, "Efficient Surface Grafting of Luminescent Silicon Quantum Dots by Photoinitiated Hydrosilylation," Langmuir **21**(13), 6054–6062 (2005).
27. I. V. Lightcap and P. V. Kamat, "Fortification of CdSe Quantum Dots with graphene oxide. excited state interactions and light energy conversion," J. Am. Chem. Soc. **134**(16), 7109–7116 (2012).
28. R. C. C. Leite and S. P. S. Porto, "Enhancement of Raman cross section in CdS due to resonant absorption," Phys. Rev. Lett. **17**(1), 10 (1966).
29. S. Zou and M. J. Weaver, "Surface-enhanced Raman scattering of ultrathin cadmium chalcogenide films on gold formed by electrochemical atomic-layer epitaxy: thickness-dependent phonon characteristics," J. Phys. Chem. B **103**(13), 2323–2326 (1999).
30. K. N. Kudin, B. Ozbas, H. C. Schniepp, R. K. Prud'homme, I. A. Aksay, and R. Car, "Raman Spectra of Graphite Oxide and Functionalized Graphene Sheets," Nano Lett. **8**(1), 36–41 (2008).
31. A. M. Bellocq, R. C. Lord, and R. Mendelsohn, "Laser-excited Raman Spectroscopy of biomolecules III. Native bovine serum albumin and beta-lactoglublin," Biochim. Biophys. Acta **257**(2), 280–287 (1972).
32. P. C. Painter and J. L. Koenig, eds., "Handbook of Biochemistry and Molecular Biology, Proteins; Raman Spectroscopy of Polypeptides and Proteins," Vol. III: pp 575–587 (1976).
33. T. M. Herne, A. M. Ahern, and R. L. Garell, "Surface-enhanced Raman spectroscopy of peptides: preferential n-terminal adsorption on colloidal silver," J. Am. Chem. Soc. **113**(3), 846–854 (1991).
34. Z. Chi, X. G. Chen, J. S. W. Holtz, and S. A. Asher, "UV resonance Raman-selective amide vibrational enhancement: quantitative methodology for determining protein secondary structure," Biochemistry **37**(9), 2854–2864 (1998).
35. P. C. Lee and D. Meisel, "Adsorption and surface-enhanced Raman of dyes on silver and gold sols," J. Phys. Chem. **86**(17), 3391–3395 (1982).
36. A. Campion and P. Kambhampati, "Surface-enhanced Raman scattering," Chem. Soc. Rev. **27**(4), 241–250 (1998).
37. S. Stewart and P. M. Fredericks, "Surface-enhanced Raman spectroscopy of peptides and proteins adsorbed on an electrochemically prepared silver surface," Spectrochim Acta A **55**(7-8), 1615–1640 (1999).
38. Z. Chen, S. Berciaud, C. Nuckolls, T. F. Heinz, and L. E. Brus, "Energy Transfer from Individual Semiconductor Nanocrystals to Graphene," ACS Nano **4**(5), 2964–2968 (2010).

#246749 Received 27 Jul 2015; revised 9 Sep 2015; accepted 9 Sep 2015; published 15 Sep 2015

1. Introduction

Non-invasive diagnosis of a disease at an early stage is essential as a therapeutic intervention, which is often simpler and more likely to be effective. To make this possible the detection of biochemical changes in bodily fluids are needed, while avoiding biopsies. The best health screening method could be the blood test because it contains thousands of biomolecules coming as by-products from the diseased part of the organism [1–3]. Two-dimensional (2D) graphene molecule made up of sp^2 hybridized carbon atoms is becoming a popular nano-system due to its unique multifunctional properties, such as large surface area [4], high thermal and electrical conductivity [5,6], and good stability. These properties make graphene more promising for its application in drug delivery and many other biological applications [7]. Since graphene has great amphiphilicity and plasmonic properties, it becomes a prominent candidate for biosensors applications. However, a lot of research is needed to manipulate graphene to work well with organic materials due to its zero-band gap [8]. Therefore, graphene oxide (GO) is proposed to be an alternative material. GO has oxygen-functional groups that allow this material to be used as a medium for covalently binding to protein molecules. This makes GO as a potential candidate for detection of biomolecules with very low detection limits [9] and specificity. However, GO is known to be a fluorescence quencher, limiting its effectiveness of its detection [10].

Quantum dots (QDs) have not only unique optical properties but also have a great potential for biological imaging, visual aids, and bio-sensing [11]. However, the major problems are that they are easily oxidized and toxic. Yet, unlike other fluorescent molecules or fluorophores, QDs have sharper photoluminescence (PL) peaks, brighter fluorescence, and are more resistant to chemical degradation [12]. Since, GO has very low fluorescence energy; the QDs donate their Forster resonance energy transfer (FRET) to GO [13] as a result the fluorescence intensity is enhanced due to the receiving of the QDs fluorescence energy by the GO. Therefore, the detection limit of the analytes is increased, making it a better biosensor, which is demonstrated in this study by using Bovine serum albumin (BSA) as the protein for detection. Semiconductor CdSe/CdS materials are used as the QDs due to their good stability, high luminescence energy, and efficient electron charge transfer [14]. Many QD-based biosensors have been developed on the basis of FRET phenomenon [13]. Similarly, the Raman spectroscopy analysis of bio fluids has the capability to serve as a standard tool at the clinical level. However, these analytes in bodily fluids pose a challenge in recording Raman spectra due to their low concentration which normally vary in the range of mmol/L to nmol/L [2, 3]. As Raman technique is an inherently weak process, the detection of small concentration of biochemical would need amplification of the Raman signal. One of the promising approaches to achieve amplified signal is the surface enhanced Raman spectroscopy (SERS) which has opened novel opportunities for chemical and biomedical analysis. SERS is a nanotechnology based phenomenon that simultaneously removes the fluorescence background and enhances the weak Raman signatures [15–17] several folds of magnitude.

In this manuscript we discuss the high quenching efficiency of GO to the fluorescence of QDs which led to high sensitivity for FRET-based bio sensing. This was further demonstrated by combining with the specific interaction between protein and its aptamer. Similarly, QDs conjugate GO enhanced Raman signals through SERS effect [18,19]. These results demonstrate the extensive application possibilities of a detection platform and open new opportunities for sensitive detection of bio-recognition events.

2. Experiment

Materials. Myristic acid (99%), 1-Octadecene (ODE, technical grade, 90%), Oleylamine (OLA, technical grade, 70%), Oleic acid (technical grade, 90%), 1-Octanediol (98.5%), 3-Aminopropyl triethoxysilane (APTAS, 98%), Cadmium oxide powder (CdO, 99.5% trace

#246749 Received 27 Jul 2015; revised 9 Sep 2015; accepted 9 Sep 2015; published 15 Sep 2015

metals basis), Selenium powder (100 mesh, 99.5%), poly (sodium 4-styrenesulfonate) (PSS, MW 70,000), dimethyl sulfide (DMSO), bovine serum albumin (BSA), sodium chloride (NaCl, 99.5%), hydrazine (1.0M solution in tetrahydrofuran), cadmium acetate hydrate, argon gas, nitrogen gas, 0.1M hydrochloric acid (HCl), deionized water, acetone, hexane, ethanol, isopropyl alcohol, 0.1M butane dithiol, and acetone nitrile. All the chemicals used were obtained from Sigma-Aldrich and were used without further purification.

Synthesis of CdSe: The quantum dots in this study are synthesized by modifying the method of Cao et al. [20] by refluxing 0.29 myristic acid, 5mL of 1-octadecene, and 0.077g of CdO at 500 mbar until the temperature reaches 240°C [21,22] The temperature and pressure are then reduced to 90° C and 44 mbar respectively after adding 32mL of ODE into the reaction. The solution is allowed to sit for approximately 1 hour and then cooled at room temperature. Next, 0.024g of the precursor selenium powder is mixed into the solution and vacuumed for 10 minutes at 50°C. Finally, the nano-crystals are grown at raising the temperature to 240° C for 1 hour in the presence of oleic acid, oleylamine, and ODE. The resulting product, an orange-red colored solution, is processed through centrifugation/sonication six times in order to remove any impurities and the final product is re-suspended in hexane.

Synthesis of Core shell, CdSe/CdS: The core shell of CdSe/CdS is synthesized by modifying the successive ion layer absorption and reaction (SILAR) protocol [21]. With the CdSe concentration being 0.08 mM, 1.13 mM of the precursor CdO is used to make the core shell. Under vacuum, CdO is introduced into a solution with 7.5 mL of oleic acid and 30mL of ODE for 1 hour before heating the solution to 240 °C. The solution is kept under vacuum for 1 hour at 44 mbar before growing the core shell at 240 °C. After the CDO is completely dissolved, the solution is kept at 80° C under nitrogen gas. The 0.1M sulfur precursor stock solution was prepared by dissolving sulfur in ODE at 180 °C. In a separate 3-neck flask, 2mL of OLA and 200uM CdSe are degassed under vacuum at 70 °C for 1 hour before the solution is heated to 230 °C under nitrogen flow. Then, the CdO solution and the sulfur solution are alternatively injected into CdSe at every ten minutes interval. The resulting product is removed of any impurities by using the same washing procedure previously stated in the synthesis of CdSe section. Next, 0.1M butane dithiol is prepared in acetone nitrile. The core shell is then capped with the butane dithiol solution to improve ligand exchange.

Preparation of Graphene Oxide (GO): The graphene oxide was prepared by oxidizing graphite following the Hummers method [23]. The GO is then coated with 88.63 mg of PSS by reducing 8.6 mg of GO with 8.6 mL of hydrazine under reflux at 115 °C (1). The solution is cleaned using centrifugation with 0.1M HCl. Next, the solution is degassed for approximately 10 minutes using argon. GO-PSS is sonicated in 0.1M HCl for two hours and then stirred for 48 hours.

Conjugation of Core Shell and Graphene Oxide: Before conjugating the core shell (CdSe/CdS) with GO coated PSS, the graphene oxide solution pH is first adjusted to a pH of 7 using 0.1M HCl. Next, 2mL of the GO coated PSS was conjugated with 2mL of the core shell using 0.2M of NaCl.

Characterizations. The UV-VIS spectra are recorded using a Perkin Elmer Lambda 950 UV-VIS-IR spectrophotometer. The Photoluminescence (PL) spectra are measured using Hitachi F-7000 fluorescence spectrophotometer. The Raman spectra are measured on a Horiba LabRam Confocal HR Evolution microRaman system with a 785 nm laser. Transmission electron microscope (TEM) images are obtained from Hitachi 4700 TEM system. Field emission scanning electron microscopy (FESEM) images are obtained from Hitachi SU81010 Scanning Electron Microscope.

3. Results and discussion

Figure 1 (a-i) shows the schematic diagram for protein detection technique using FRET mechanism. The photo-excited fluorescent energy is transferred from CdSe/CdS QDs to GO

#246749 Received 27 Jul 2015; revised 9 Sep 2015; accepted 9 Sep 2015; published 15 Sep 2015

suffering the quenching of PL through FRET, and consequently enhancing the imaging of biomolecules, such as BSA. Optical surface morphology studies of GO-PSS and QD-conjugate-GO-PSS are shown in Fig. 2. During the process of functionalization of QDs with GO-PSS, we first coated graphene oxide with PSS, which is shown in Fig. 2(a). GO-PSS exhibits a three-dimensional network of randomly oriented plate-like structures with a wrinkled texture and hierarchical pores with a wide size distribution. From the top-view image, the composites have a uniform and dense surface, composed of particles with slightly scrolled edges ranging from several tens of nanometers to several hundreds of nanometers in the lateral dimension. This image shows evidence that the PSS is well attached and assembled onto the graphene oxide surface. FESEM image of QD-conjugated-GO-PSS are shown in Fig. 2(b).

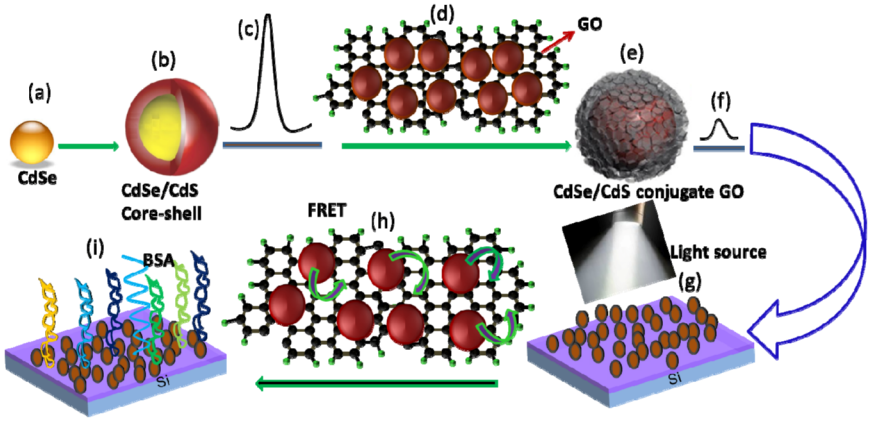

Fig. 1. (a)-1(i) shows the schematic diagram for protein detection technique using FRET mechanism. Figure 1(a) to 1(c) represents the image of nano-crystals of CdSe, CdSe coated with CdS QDs and its sharp PL obtained from the core shell of CdSe/CdS QDs, respectively. Figure 1(d) and 1(e) show the conjugation of core shell with GO as a result of quenching of the PL peak observed due to strong absorption of GO towards the excited light source (Fig. 1(f)). Figure 1(g) represents the distribution of core shell conjugated GO onto the Si substrate with illumination of laser source. Fig. 1(g)-1(h) signify the photo-excited fluorescent energy that is transferred from CdSe/CdS QDs to GO suffering from the quenching of PL through FRET, and consequently enhancing the imaging of biomolecules, such as BSA.

#246749 Received 27 Jul 2015; revised 9 Sep 2015; accepted 9 Sep 2015; published 15 Sep 2015

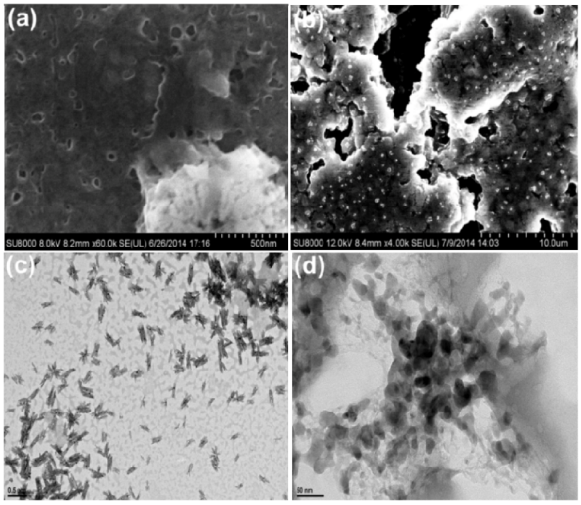

Fig. 2. (a) FESEM image of GO-PSS, (b) QD-conjugate-GO-PSS, (c) -(d) TEM images of GO-PSS.

The FESEM image illustrates that well-defined spherical QD core shell with uniform average particle sizes distribution of 5 nm are assembled with GO-PSS. The surface is much rougher and distinctly enfolded with gauze-like structure and can be attributed to the covalent linkage of QDs with GO-PSS sheet. TEM image of GO-PSS with different magnification are shown in Fig. 2 (c) and 2 (d). It is seen that, GO sheet is well distributed in PSS matrix which favors to formation of QD-conjugate-GO-PSS by the subsequent addition of QDs during chemical process.

Figure 3 shows the TEM images of QDs core shell, Graphene oxide and of QD conjugated GO-PSS for different magnification. From TEM image it is seen that the QDs core shell are spherical in shape and uniformly distributed on the surface. Similarly, TEM image of Graphene oxide is highly electron transparent even in comparison to the thin-film of carbon. However, the contrast dark image shows the overlapping of few layers of graphene oxide sheet. Furthermore TEM (Fig. 3 (c) and 3 (d)) images with different magnification provided direct evidence for the well-assembled QDs and the conjugation of the QDs conjugate-GO-PSS. The HRTEM image clearly showed well-defined individual CdSe/CdS QDs (Fig. 3(d)), in the GO-PSS matrix. Moreover, the average size of individual CdSe/CdS QDs was estimated to be 4-5 nm.

#246749 Received 27 Jul 2015; revised 9 Sep 2015; accepted 9 Sep 2015; published 15 Sep 2015

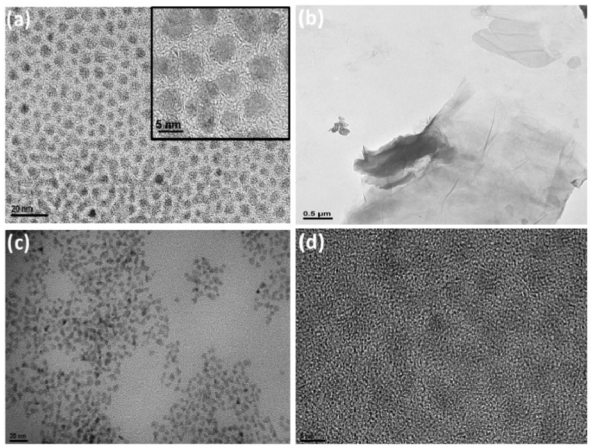

Fig. 3. (a) TEM image of CdSe/CdS (Inset shows high magnification), (b) TEM image of QD conjugated GO-PSS, (c) TEM image of QD conjugated GO-PSS, (d) TEM image of QD conjugated GO-PSS 5nm magnification.

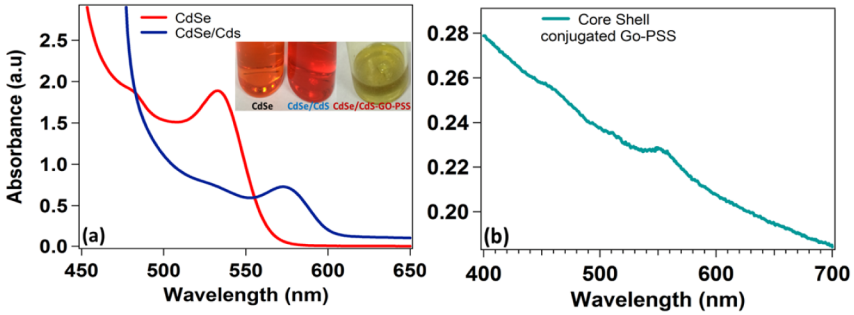

Fig. 4. The UV-VIS absorption Spectra of CdSe, CdSe-CdS and core shell conjugated GO-PSS. Insertion: photograph of respective solution.

The UV–VIS absorption spectra were also used to characterize the formation of CdSe QDs, core shell (CdSe/CdS) and the QD conjugated GO -PSS are shown in Fig. 4. The CdSe QDs and CdSe/CdS core shell displayed well-resolved maxima in absorption peak at about 537nm and 555nm, respectively, indicating a sufficiently narrow size distribution of the QDs. The result was also confirmed by the PL spectra. The observed darker reddish color in the CdSe/CdS core shell solution as compared to CdSe solution indicates the successful coating of CdSe QDs by CdS. As a result, its absorption peak is shifted towards higher wavelength region (red shift), representing a larger particle size besides a well-assembled core shell. However, the appearance of broad absorption peak after modification of the core shell (core shell-conjugated GO-PSS) decreased from 2.0 to 0.23, which provides strong evidence for quenching of the quantum dots by GO. Furthermore, a red shift is observed from 555 nm to 560 nm, indicating a successful conjugation due to the bigger particle size.

Degree of oxidation within the chemically exploited graphene was used to isolate the influence of the electron transfer pathway during excited state deactivation of CdSe/Cds QDs by GO in QDs conjugate-GO-PSS composite. Since GO is an extremely good electron acceptor, it has a strong capability to consume more electrons due to its oxidation state. This behavior of GO is more favorable for the fluorescence quenching of CdSe/CdS core-shell as a probe to distinguish the extent of excited state electron transfer to GO [24]. Photoluminescence spectra of CdSe, CdSe/CdS and QD conjugate-GO-PSS composite are shown in Fig. 5. The PL spectrum of CdSe QDs shows a strong peak at 576 nm. In the

#246749 Received 27 Jul 2015; revised 9 Sep 2015; accepted 9 Sep 2015; published 15 Sep 2015

meanwhile, the characteristic peak intensity in the PL spectrum of the core shell of CdSe/CdS decreases and shifts towards higher wavelength (red shift) region as compared to the CdSe QDs. However, the PL intensity of QDs conjugate-GO-PSS suppresses drastically, about 95% of the original intensity of CdSe QDs. The shift of PL peak position of CdSe/CdS and QDs conjugate-GO-PSS is mainly attributed to the change of the surface charge as well as charge transfer of QDs upon GO-PSS modification [25, 26].

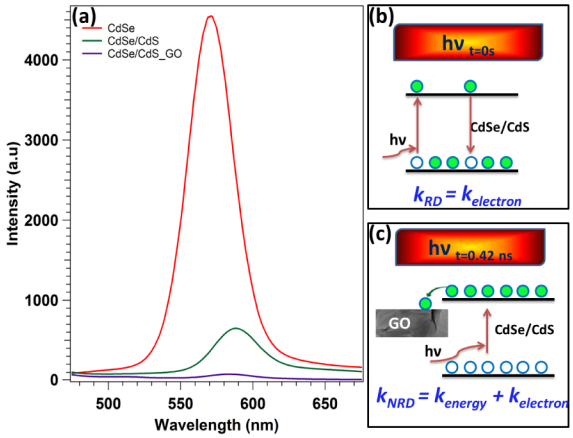

Fig. 5. (a) The PL spectra of CdSe, CdSe/CdS and CdSe/CdS conjugated GO, (b) Schematic PL spectra of core shell QDs, (c) Initial illumination of CdSe/CdS conjugated GO leads to electron transfer from core shell conduction band to GO.

The strong interactive characteristic of GO reveal that GO serve as effective quenchers of excited CdSe/CdS core-shell even at the smallest GO concentrations. The degree of energy transmission between the donor (CdSe/CdS) and the acceptor GO is dependent on the proximity as well as spectral overlap between the two compounds which most likely the consequence of GO's electron accepting ability combined with its highly interactive nature. The charge transfer events between photoexcited QDs and GO can sequentially be explained as follows. We have taken into account the example of CdS/CdSe core-shell system as one described for CdSe QDs [27].

$$\mathrm{CdS/CdSe} = \mathrm{h}\vartheta \rightarrow \mathrm{CdS/CdSe(e+h)}.. \quad (1)$$

$$\mathrm{CdS/CdSe(e)} + \mathrm{GO} \rightarrow \mathrm{CdS/CdSe} + \mathrm{GO(reduced)}.. \quad (2)$$

$$\mathrm{CdS/CdSe(e)} + \mathrm{GO(R)} \rightarrow \mathrm{CdSe} + \mathrm{GO}\left(\mathrm{R}\right)\mathrm{(e)}.. \quad (3)$$

The quenching of photoluminescence of QDs by GO follows the above three steps as, reduction and electron storage and quenching by GO. The electron transfer and/or energy transfer of the excited state of the QDs are responsible for the quenching of emission.

#246749 Received 27 Jul 2015; revised 9 Sep 2015; accepted 9 Sep 2015; published 15 Sep 2015

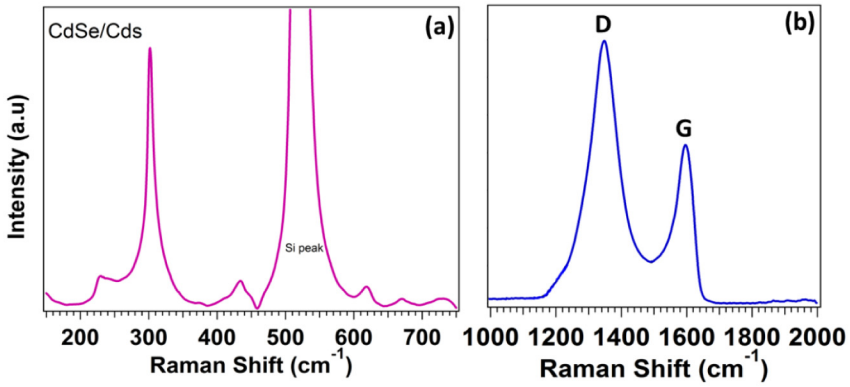

Fig. 6. (a) The Raman Spectra of CdSe/CdS core shell on a silicon substrate, (b) Raman Spectra of Graphene oxide.

In the core shell of CdSe/CdS QDs, CdSe QDs with a diameter of 3.8 nm have been used as cores for the core shell NCs. In order to study the more complicated core shell system for the analysis of the core features, Raman spectra of the sample is taken with an excitation wavelength of 785 nm CdSe/CdS core shell NCs as shown in Fig. 6(a). The TO mode of CdSe QDs is not observed in core shell structures because all the core-related Raman features have lower intensity in core shell QDs due to strong absorbance of the shell at the excitation wavelength. The Raman band for CdSe QDs with the core shifts to higher frequency due to capping by CdS shell. It is recognized to the scattering of CdSe longitudinal optic phonons; the peak at 228.8 cm^{-1} is noticeable as LO. In addition to the first-order Raman line, the high-order Raman peaks are also observed showing a difference mode: 2LO1, the second-order phonon frequency of CdSe around 425cm^{-1} and also the overtones of the longitudinal optical phonon around 611 cm^{-1} (3LO1). Similarly, the frequency of the Raman active LO phonon in CdS is shifted down to 300 cm^{-1} from 305 cm^{-1} as compare to its bulk counterpart [28] represents the thin layer of superlattices by the combined effect of strain and phonon confinement [29].

Figure 6(b) shows the Raman spectra in the region 1100-1800 cm^{-1} for GO. As expected, GO shows a broadened and blue-shifted G band at 1590 cm^{-1} and a broad, intense peak at 1330 cm^{-1}, the disorder-induced D band. The blue-shifted, broadened G band and intense D band are consistent with previous Raman investigations of GO [30] and are indicative of the severe disruption or disorder induced into the sp^2 carbon lattice by the oxidative synthesis of GO.

Raman spectroscopy is an essential tool for the structure determination of the biomolecules. The effects of fluorescence and lower sensitivity on the normal Raman spectra of these molecules make more difficulties to identify the proper structure which led to the extension of research in more appropriate way to enhance the Raman signal. Hence, surface enhanced Raman scattering (SERS) effect favor to recognize the fingerprint of different biomolecules more efficiently. Albumin is the most abundant protein in the circulatory system and contributes 80% to colloid osmotic blood pressure. The Raman spectra of BSA on core shell in the spectral range of 600–1700 cm^{-1} are presented in Fig. 7. The spectral region between 1200 and 1300 cm^{-1} is poorly represented, indicating the dominant presence of a-helix content. The secondary structure of BSA (a helix, b-pleated sheet, and random coil) is observed in the Raman spectra through the contribution of strong amide I band (1656 cm^{-1}) and weak amide III band (1270 cm^{-1}) [31–34]. Similarly, bands at 1007, 1027, and 1604 cm^{-1} are corresponding to the phenyl stretching mode shown in the Raman spectra, indicates the aromatic amino acid residues. The scissoring modes of CH_2 and CH_3 are located at 1447 and 1462 cm^{-1}, respectively. Moreover, the bands from the side chains of some of the amino acids

#246749 Received 27 Jul 2015; revised 9 Sep 2015; accepted 9 Sep 2015; published 15 Sep 2015

residues (tyrosine, tryptophan, phenylalanine, etc.) are present. Besides the common amide bands, the supplementary disulfide bridges are characteristic for BSA [35]. The characteristic frequencies of COS and SOS groups are present as weak–medium bands in the 600–750 cm^{-1} spectral region.

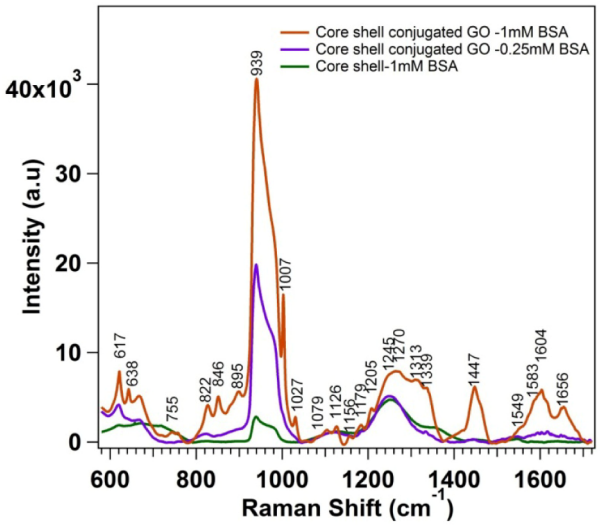

Fig. 7. The Raman spectra of core shell with 1mM BSA, core shell conjugate GO-0.25 and 1mM BSA.

However, GO conjugate core shell BSA is strongly enhance from their corresponding Raman spectra (Fig. 7) in both the band positions and relative intensities even at the very low concentration of BSA (0.25mM). These differences could have at least two possible explanations: SERS and normal Raman probably span a different portion of the protein structure, and thus the bands of different wavenumbers and relative intensities are observed; further, based on SERS theory [33,36], the molecules can be physisorbed or chemisorbed, the last case being characterized through the drastic spectral change on passing from Raman to SERS. When the chemisorption takes place, the molecule of interest together with the nanometric surface builds a socalled "Core shell conjugate graphene oxide–molecule SERS complex" where a charge transfer contribution to the total enhancement mechanism [36] is present. The amide I bands corresponding to the a-helix, b-sheet, and random coil conformations occur in the 1640-1658, 1665-1680, and 1660-1666 cm^{-1} ranges [37], respectively. On the other hand, the amide III band positions of these conformations were localized in the 1260-1310, 1235-1242, and 1240-1250 cm^{-1}regions, respectively.

The QDs exhibit a variety of advantages, such as high quantum yield due to strong photolumescence; narrow, symmetric and stable fluorescence; and size-dependent and tunable absorption and emission. Owing to broad absorption and narrow emission spectra the QDs are excellent donors of fluorescence for FRET. The excited state decay from photogenerated electrons in QDs or Ncs on adjacent entities can takes place via FRET [38]. Relaxation via this pathway does not involve electron transfer and hence it is very effective to a semiconductor NCs and GO composite system designed for improved electron transfer. The FRET between QDs and GO and the strong interaction between the biomolecules and GO can be combined to develop a novel ultrasensitive and selective platform for fluorescence-quenching detection of biomolecules. Therefore, Emission decay traces of CdSe/CdS and CdSe/CdS-GO composites shown in Fig. 8. It is observed that, the CdSe/CdS PL lifetimes (8.53ns) is more and nearly constant as excited state electron transfer from CdSe is very slow. However, in case of CdSe/CdS-GO composite, the PL lifetime (0.42ns) is observed to be very

#246749 Received 27 Jul 2015; revised 9 Sep 2015; accepted 9 Sep 2015; published 15 Sep 2015

little and approximately 20 times less than the CdSe/CdS QDs. Hence, with the electron transfer pathway unavailable, PL lifetimes necessarily increase as energy transfer becomes the only available route for conduction band electrons undergoing non-radiative excited state decay. This effect is confirmed by the increasing PL lifetimes observed in core shell QDS composites with prolonged visible light irradiation.

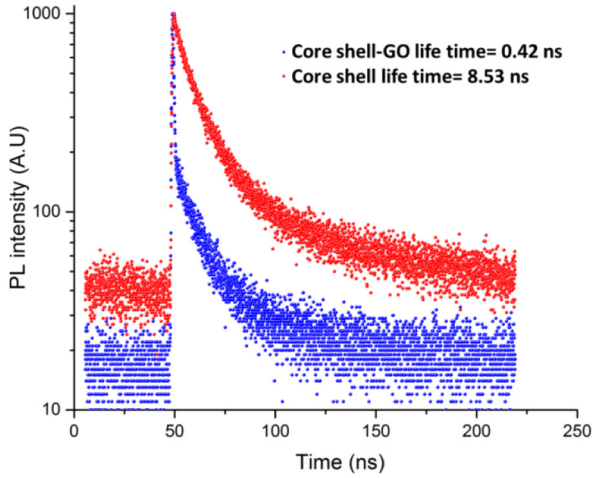

Fig. 8. Photoluminescence lifetimes of Core shell and Core shell conjugated GO .

4. Conclusion

We have demonstrated the detection of low concentrations of protein using core shell conjugated graphene oxide as a new biosensor. Our experimental results are evidence of the fact that GO is the most powerful acceptor of QDs FRET donors. The demonstrated properties can be of exceptional importance for several kinds of applications in nano-biotechnology. The Raman spectroscopy data demonstrated that the QDs -GO conjugation can detect low concentration of BSA at a higher intensity compared to BSA on a silicon substrate. The data suggests that this novel dual nanoparticle system integrates the advantages of both QDs and GO and demonstrates a very promising future for not only detecting proteins but also being functionalized for selectivity for specific biomolecules with a low detection limit. With the high fluorescence energy of QDs being used as a donor for GO, only low concentrations of QDs and GO are needed for an efficient bio-sensing. The application of such GO based QD-FRET quenching platforms may bring new advantages in the analytical performance of future bio-sensing systems beside opening the door to the design of novel sensing strategies with interest for diagnostics, safety and security, environmental and other industrial applications. The QDs fluorescence quenching by GO may open unprecedented imaging flexibility and become a general tool for characterizing graphene based materials for several other applications. It can also be extended to several other fluorescent materials with interest for optoelectronic or bio-sensing applications.

Acknowledgments

This work is supported by the NSF-CREST (CNBMD) Grant number HRD 1036494 and NSF-RISE. The authors are thankful to H. Yoon for relaxation experiment.

#246749 Received 27 Jul 2015; revised 9 Sep 2015; accepted 9 Sep 2015; published 15 Sep 2015